Title
Communication: Atomic force detection of single-molecule nonlinear optical vibrational spectroscopy

Journal
The Journal of Chemical Physics, 140(16)

ISSN
0021-9606

Authors
Saurabh, Prasoon
Mukamel, Shaul

Publication Date
2014-04-28

DOI
10.1063/1.4873578

Peer reviewed

Communication: Atomic force detection of single-molecule nonlinear optical vibrational spectroscopy

Prasoon Saurabh and Shaul Mukamel

Citation: The Journal of Chemical Physics **140**, 161107 (2014); doi: 10.1063/1.4873578
View online: http://dx.doi.org/10.1063/1.4873578
View Table of Contents: http://scitation.aip.org/content/aip/journal/jcp/140/16?ver=pdfcov
Published by the AIP Publishing

Communication: Atomic force detection of single-molecule nonlinear optical vibrational spectroscopy

Prasoon Saurabh[a] and Shaul Mukamel[b]
Department of Chemistry, University of California, Irvine, California 92697, USA

(Received 6 March 2014; accepted 14 April 2014; published online 30 April 2014)

Atomic Force Microscopy (AFM) allows for a highly sensitive detection of spectroscopic signals. This has been first demonstrated for NMR of a single molecule and recently extended to stimulated Raman in the optical regime. We theoretically investigate the use of optical forces to detect time and frequency domain nonlinear optical signals. We show that, with proper phase matching, the AFM-detected signals closely resemble coherent heterodyne-detected signals. Applications are made to AFM-detected and heterodyne-detected vibrational resonances in Coherent Anti-Stokes Raman Spectroscopy ($\chi^{(3)}$) and sum or difference frequency generation ($\chi^{(2)}$). © *2014 AIP Publishing LLC*. [http://dx.doi.org/10.1063/1.4873578]

Atomic force microscopy of single molecules has seen many advancements over the past two decades since its theoretical and experimental advents in early 1990s.[1,2] Optical forces have been used to create optical lattices for trapping cold atoms and ions.[3] Magnetic and optical tweezers are versatile tools for measurements of forces and corresponding single molecule displacements in biological molecules such as DNA and proteins. AFM measurements provide high resolution and conformational control of bio-macromolecules. Non-contact AFM has been used to visualize intermolecular bonds such as hydrogen bonds.[4] Magnetic tweezers are often used for analysing DNA topology, and like optical tweezers, can perform 3-dimensional manipulations. These techniques generally measure the displacement of molecular position caused by the forces applied by the probe.[5–11] The optical potential acting on the single molecule by the fields can trap cold atoms in optical lattices.[3] Measuring its gradient (the force) constitutes a new type of signal.

Here we theoretically investigate how optical forces may be used to detect nonlinear optical signals. Instead of measuring the mechanical displacement of single molecule induced by the applied force, one can look at the gradient force applied by the AFM tip to the molecule.[12,13] In such measurements, the spectroscopic information is contained in the pulse parameters used to create the force. Stimulated Raman resonances related to $\chi^{(3)}$ have been recently reported experimentally by Rajapksa *et al.*[22] The mechanical force associated with different NonLinear Optical (NLO) techniques like FRET-force in force imaging has been investigated.[14] A plethora of methods have been employed for detecting nonlinear optical signals. These include homo and hetrodyne detection of fields,[15,16] incoherent fluorescence detection,[17,18] photoacoustic detection,[19,20] photoelectron, and current detection.[21]

We derive general expressions for ultrafast nonlinear optical spectroscopy with gradient force detection. A single molecule on a glass cover slide is subjected to several collinear laser beams and the variation of the gradient force with selected parameters such as delays between pulses, phases, or frequencies is measured by AFM tip using vibrational tapping mode,[22] thus generating multidimensional signals. We show that by manipulating the phases between fields, it is possible in some cases to make the optical potential (and gradient force) to coincide with the heterodyne signal.[23]

The conservative force is given by the gradient of the optical potential $\mathbf{V}(\mathbf{r})$.[3,12,14]

$$\mathbf{F}(\mathbf{r})_{\mathbf{gr}} = -\nabla_{\mathbf{r}}\mathbf{V}(\mathbf{r}). \tag{1}$$

We first calculate the potential felt by the molecule due to its nonlinear coupling to electromagnetic fields in continuous wave (cw) frequency-domain experiments.[24] n classical monochromatic fields induce a polarization $\mathbf{P}(\omega)$ in the molecule, which then creates an optical potential ($\mathbf{V}$),[23]

$$\mathbf{V}(\mathbf{r}) = -\Re\big[\int d\omega \mathbf{P}(\omega).\mathbf{E}^*(\mathbf{r},\omega)\big] = -\Re\big[\int dt \mathbf{P}(t).\mathbf{E}^*(\mathbf{r},t)\big]. \tag{2}$$

The classical electric field can be expanded in modes:

$$\mathbf{E}_i(\mathbf{r},t) = \sum\nolimits_{\xi_i=\pm} \epsilon_i \int \frac{d\omega_i}{2\pi} \mathcal{E}_i^{\xi_i}(\mathbf{r},\omega_i) e^{i\xi_i(\omega_i t+\phi_i)},$$
$$\mathbf{E}_i(\mathbf{r},\omega) = \sum\nolimits_{\xi_i=\pm} 2\pi.\epsilon_i \mathcal{E}_i^{\xi_i}(\mathbf{r},\omega_i) e^{i\xi_i\phi_i}\delta(\omega' - \xi_i\omega), \tag{3}$$

where $\mathcal{E}_i^{\xi_i}(\mathbf{r},\omega)$ is the position dependent envelope of the ith field and $\xi_i = \pm$ is the hermiticity (negative for positive frequency and positive for negative frequency component) of the field. ϕ_i is the phase angle between the incident classical field modes and ϵ_i is the respective polarization vector. The optical potential is given by

$$\mathbf{V}(\mathbf{r}) = -\Re\int_0^\infty d\omega \mathbf{P}(\omega).\mathbf{E}^*(\mathbf{r},\omega), \tag{4}$$

where $\omega > 0$. For comparison, the heterodyne detected signal measured at ω' is given by[25]

$$S(\mathbf{r};\omega') = -\Im\int_0^\infty d\omega \mathbf{P}(\omega).\mathbf{E}^*(\mathbf{r},\omega). \tag{5}$$

[a]Electronic mail: psaurabh@uci.edu
[b]Electronic mail: smukamel@uci.edu

The total induced polarization is the sum of positive and negative frequency components, $\mathbf{P}_{total}(\omega) = \mathbf{P}^{+}(\omega) + \mathbf{P}^{-}(\omega)$. One can identify $\mathbf{P}^{+}(\omega)$ with $\mathbf{P}(\omega)$ and $\mathbf{P}^{-}(\omega)$ with $\mathbf{P}^{*}(\omega)$. Similarly, we can identify $\mathbf{E}^{+}(\omega)$ with $\mathbf{E}(\omega)$ and $\mathbf{E}^{-}(\omega)$ with $\mathbf{E}^{*}(\omega)$. The superscripts + and − denote the positive or negative frequency components. For a cw measurement involving discrete set of modes, we have

$$\mathbf{V}_d(\mathbf{r};\omega_j) = -\Re \sum_j \mathbf{P}(\omega_j).\mathbf{E}^{*}(\mathbf{r},\omega_j), \tag{6}$$

$$S_d(\mathbf{r};\omega_j') = -\Im \sum_j \mathbf{P}(\omega_j).\mathbf{E}^{*}(\mathbf{r},\omega_j). \tag{7}$$

For the linear response, we get the optical potential and heterodyne signal,

$$\mathbf{V}^{(1)}(\mathbf{r};\omega_j) = -\sum_j \chi^{(1)'}(\omega_j).|\mathbf{E}(\mathbf{r},\omega_j)|^2, \tag{8}$$

$$S^{(1)}_{het}(\mathbf{r};\omega_j) = -2\sum_j \chi^{(1)''}(\omega_j).|\mathbf{E}(\mathbf{r},\omega_j)|^2, \tag{9}$$

where, linear susceptibility, $\chi^{(1)}(\omega) = \chi^{(1)'}(\omega) + i\chi^{(1)''}(\omega)$. Superscripts $'$ and $''$ denote the real and imaginary part. For a multilevel system, we have

$$\chi^{(1)}(\omega) = \frac{1}{\hbar}\sum_{a,c} P(a)\frac{|\mu_{ac}|^2\omega_{ac}}{(\omega_{ac})^2 - (\omega + i\Gamma_{ac})^2}, \tag{10}$$

where, $P(a) = e^{-\beta\varepsilon_a}/\sum_a e^{-\beta\varepsilon_a}$ with ε_a as the eigen energy of level a, and $\beta = 1/k_bT$ with temperature T. The linear optical potential and heterodyne signal have dispersive and absorptive profiles at $\omega = \omega_{ac}$ as depicted in Fig. 1.

We now turn to a second order process (Fig. 2) where ω_1 in the IR regime, ω_2 and ω_3 are in visible region , and $\omega_3 = \omega_1 + \omega_2$, the optical potential is then given by

$$\mathbf{V}^{(2)}(\mathbf{r};\omega_1,\omega_2) = -\Re\Big[\sum_j (2\pi)^3\mathcal{E}_1(\mathbf{r},\omega_j)\mathcal{E}_2(\mathbf{r},\omega_j) \mathcal{E}_3^{*}(\mathbf{r},\omega_j)\sum_p\{\chi^{(2)}(-\omega_3;\omega_1,\omega_2)\}\Big], \tag{11}$$

where, $\sum_p$ represents the sum over all permutations of frequencies $\{\omega_1, \omega_2, -\omega_3\}$.$\chi^{(2)}(-\omega_3;\omega_1,\omega_2)$ represents Sum Frequency Generation (SFG) whereas the other two permutations, when ω_2 or ω_1 are detected, are Difference Frequency Generation (DFG). All possible processes contribute to the optical potential. The total heterodyne-detected signals is:

$$S^{(2)}_{total}(\mathbf{r},\omega_3;\omega_1,\omega_2) = -\Im\Big[\sum_j (2\pi)^3\mathcal{E}_1(\mathbf{r},\omega_j) \mathcal{E}_2(\mathbf{r},\omega_j)\mathcal{E}_3^{*}(\mathbf{r},\omega_j)\sum_p \chi^{(2)}(-\omega_3;\omega_1,\omega_2)\Big]. \tag{12}$$

Using the level scheme of Fig. 2 and invoking the Rotating Wave Approximation (RWA), we obtain,

$$\mathbf{V}^{(2)}(\mathbf{r};\omega_1,\omega_2) = -\Re\Bigg[\frac{-i}{2\hbar^2}\sum_j (2\pi)^3\mathcal{E}_1(\mathbf{r},\omega_j) \mathcal{E}_2(\mathbf{r},\omega_j)\mathcal{E}_3^{*}(\mathbf{r},\omega_j)\mu_{ac}\mu_{cb}\mu_{ba}\sum_a P(a) \Bigg\{\frac{1}{(\omega_{IR} - \omega_{ca} + i\Gamma_{ca})(\omega_{IR} + \omega^{(2)}_{vis} - \omega_{ab} + i\Gamma_{ab})} + \frac{1}{(\omega^{(3)}_{vis} - \omega_{ab} + i\Gamma_{ab})}\Bigg(\frac{-1}{(\omega^{(3)}_{vis} - \omega^{(2)}_{vis} - \omega_{ac} + i\Gamma_{ac})} + \frac{1}{(\omega^{(3)}_{vis} - \omega^{(1)}_{IR} - \omega_{ca} + i\Gamma_{ca})}\Bigg)\Bigg\}\Bigg]. \tag{13}$$

The sum of the three heterodyne signals (Eq. (12)) is given by replacing $\Re$ with $\Im$ in Eq. (13) as shown in Fig. 3.

We next turn to the third order optical potential and heterodyne signal (measured at ω_4) for a four wave mixing of

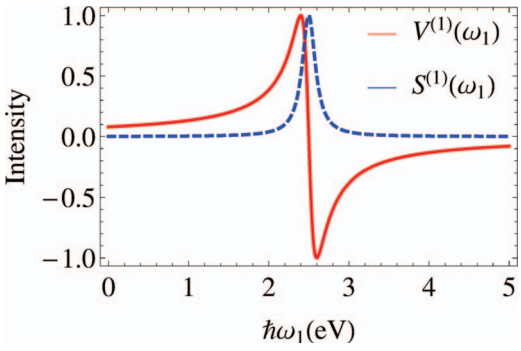

FIG. 1. Optical potential (solid red) and heterodyne signal (dashed blue) induced on single chromophore at $\hbar\omega_{ac} = 2.5$ eV using real and imaginary part of Eq. (10)

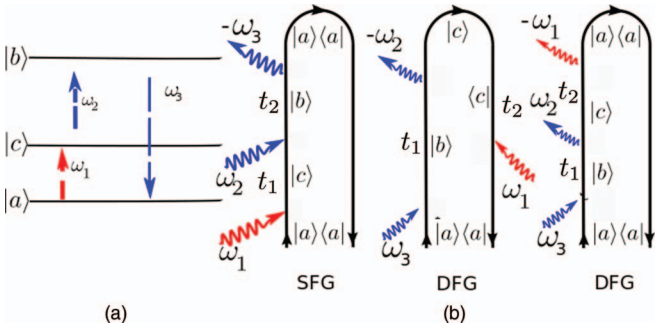

FIG. 2. (a) The three level model scheme used to calculate the $\chi^{(2)}$ optical potential and heterodyne signal. (b) Loop diagram for SFG and DFG associated to the level diagram in Fig. 2(a)

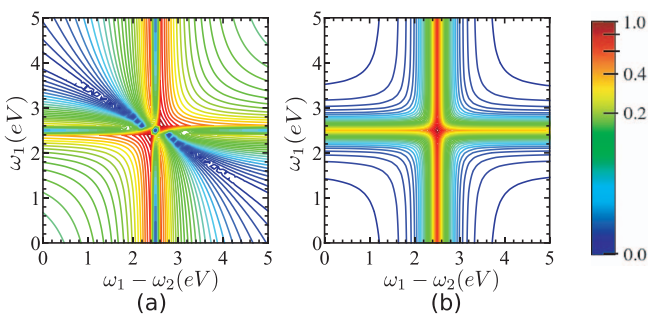

FIG. 3. (a) Optical potential Eq. (13) for cw $\chi^{(2)}$ with $\mu_{ac} = 6D$, $\mu_{bc} = 1D$, ω_{ac}=2.3 eV, ω_{ba}=10 eV, ω_{bc}=10 eV, Γ_{ac}=5 cm^{-1}, Γ_{bc}=5 cm^{-1}, and $\Gamma_{ab} = 5$ cm^{-1}. (b) Total heterodyne signal (SFG+DFG) for the same parameters.

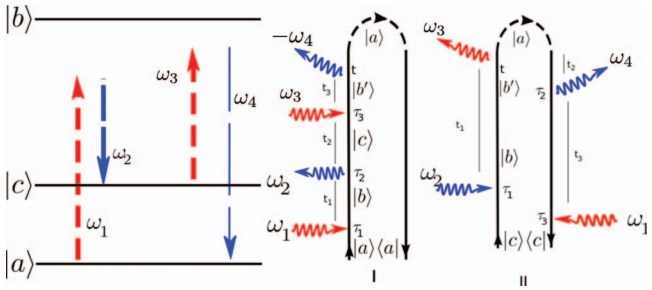

FIG. 4. The three level model system used to calculate the optical potential and heterodyne $\chi^{(3)}$ signal and the contributing Unrestricted loop diagram.

configuration $\omega_4 = \omega_1 - \omega_2 + \omega_3$ as shown in Fig. 4, at resonance frequency $\omega_1 - \omega_2 = \omega_{ac}$ and coherent fields $(-sgn(\omega_j)\sum_i \phi_i = 0)$ are given by

$$\mathbf{V}^{(3)}(\mathbf{r};\omega_1,-\omega_2,\omega_3) = -\Re\Big[\sum_j (2\pi)^4 \mathcal{E}_1(\mathbf{r},\omega_j)\mathcal{E}_2^*(\mathbf{r},\omega_j) \mathcal{E}_3(\mathbf{r},\omega_j)\mathcal{E}_4^*(\mathbf{r},\omega_j)\sum_p\{\chi^{(3)}(-\omega_4;\omega_1,-\omega_2,\omega_3)\}\Big], \tag{14}$$

$$S_{het}^{(3)}(\mathbf{r},\omega_4;\omega_1,-\omega_2,\omega_3) = -\Im\Big[\sum_j (2\pi)^4 \mathcal{E}_1(\mathbf{r},\omega_j)\mathcal{E}_2^*(\mathbf{r},\omega_j) \mathcal{E}_3(\mathbf{r},\omega_j)\mathcal{E}_4^*(\mathbf{r},\omega_j)\chi^{(3)}(-\omega_4;\omega_1,-\omega_2,\omega_3)\Big]. \tag{15}$$

For the three level system shown in Fig. 4, with ground state (a), vibrational excited state (c) and electronic excited state (b), the CARS resonances of $\chi^{(3)}$ for $(\omega_4 = \omega_1 - \omega_2 + \omega_3)$ is[25]

$$\chi_{CARS}^{(3)}(-\omega_4;\omega_1,-\omega_2,\omega_3) = \frac{P(a)|\mu_{ba}|^2|\mu_{ac}|^2}{(\omega_1-\omega_{ba}+i\eta_e)} \frac{1}{(\omega_1-\omega_2+\omega_3-\omega_{bc}+i\eta_e)(\omega_1-\omega_2-\omega_{ac}+i\eta_R)}. \tag{16}$$

Unlike the heterodyne signal which is measured at a selected frequency, the optical potential Eq. (14) is given by a sum over all possible permutations of signal frequency for $\chi^{(3)}$. The two signals coincide if we change the overall phase of $\mathcal{E}_1(\mathbf{r},\omega_j)\mathcal{E}_2^*(\mathbf{r},\omega_j)\mathcal{E}_3(\mathbf{r},\omega_j)\mathcal{E}_4^*(\mathbf{r},\omega_j)$ by $\frac{\pi}{2}$ and assume the Rotating Wave Approximation (RWA) as was done in deriving Eq. (13) for $\chi^{(2)}$.

Consider a special case involving only two fields with frequencies ω_1 and ω_2, $\mathcal{E}_3(\mathbf{r},\omega_j) = \mathcal{E}_1(\mathbf{r},\omega_j)$ and $\mathcal{E}_2(\mathbf{r},\omega_j) = \mathcal{E}_4(\mathbf{r},\omega_j)$, we can rewrite Eqs. (14) and (15) as

$$\mathbf{V}^{(3)}(\mathbf{r};\omega_1,-\omega_2) = -\sum_j (2\pi)^4 |\mathcal{E}_1(\mathbf{r},\omega_j)|^2 |\mathcal{E}_2(\mathbf{r},\omega_j)|^2 \sum_p\{\chi^{(3)'}(-\omega_2;\omega_1,-\omega_2,\omega_1)\}, \tag{17}$$

$$S_{total}^{(3)}(\mathbf{r};\omega_1,-\omega_2) = -\sum_j (2\pi)^4 |\mathcal{E}_1(\mathbf{r},\omega_j)|^2 |\mathcal{E}_2(\mathbf{r},\omega_j)|^2 \sum_p\{\chi^{(3)''}(-\omega_2;\omega_1,-\omega_2,\omega_1)\}. \tag{18}$$

AFM provides the same information as heterodyne detection but with a much higher sensitivity ($\sim pN$ *force*) that allows to detect single molecules [SI from Ref. 22]. If the relevant field factors are real, for example, in linear regime or in Eqs. (17) and (18), then the heterodyne signal is given by imaginary part of susceptibility (χ'') and the optical potential (and gradient force) is given by the real part of susceptibility (χ'). In some cases, it is possible to vary the phases and make the optical potential (or gradient force) coincide with the heterodyne signal.

We now apply the results to the three-level model system shown in Fig. 4, with ground state (a), vibrational excited state (c), and electronic excited state (b),$\chi^{(3)}$ for stimulated CARS for two beam $(\omega_4 = 2\omega_1 - \omega_2)$ within the RWA is[25]

$$\chi_{CARS}^{(3)}(-\omega_2;\omega_1) = \frac{P(a)|\mu_{ba}|^2|\mu_{ac}|^2}{(2\omega_1-\omega_2-\omega_{ab'}+i\eta_{ab'})} \frac{1}{(\omega_1-\omega_2-\omega_{ac}+i\eta_{ac})(\omega_1-\omega_{ba}+i\eta_{ba})}, \tag{19}$$

$$\chi_{CARS}^{(3)}(-\omega_1;\omega_2) = \frac{P(c)|\mu_{ba}|^2|\mu_{ac}|^2}{(2\omega_2-\omega_1-\omega_{ac}+i\eta_{ac})} \frac{1}{(\omega_2-\omega_1-\omega_{bb'}+i\eta_{bb'})(\omega_2-\omega_{cb}+i\eta_{cb})}. \tag{20}$$

Since the electronic transition frequencies ω_{bc} and ω_{ab} are much higher than the vibrational frequency ω_{ac}, we can rewrite Eq. (16) for optical potential as, Eq. (21), where $\chi_\Sigma^{(3)} = \Re[\sum_p \chi_{CARS}^{(3)}(-\omega_2;\omega_1)]$. We get the total heterodyne signal by simply replacing $\Re$ in Eq. (21) with $\Im$,

$$\mathbf{V}^{(3)}(\mathbf{r};\omega_1,-\omega_2) = -\Big[\sum_j (2\pi)^4 |\mathcal{E}_1(\mathbf{r},\omega_j)|^2 |\mathcal{E}_2(\mathbf{r},\omega_j)|^2 \chi_\Sigma^{(3)}\Big]. \tag{21}$$

Raman resonances are observed when $\omega_1 - \omega_2 = \pm\omega_{ac}$ where ω_{ac} is the difference between two ground vibrational states. The calculated optical potential and heterodyne signals are shown in Fig. 5. The gradient force due to this Raman resonance was calculated in Ref. 22 using phenomenological nonlinear polarizability. Our expression is recast in terms of the general third order polarizability $\chi^{(3)}$ and allows to calculate the optical potential (or gradient force) for other techniques as well.

We next turn to time-domain measurements which use temporally well separated impulsive pulses. The induced nth order optical potential $\mathbf{V}(\mathbf{r};t_j)$ and heterodyne signal $S(\mathbf{r};t_j)$

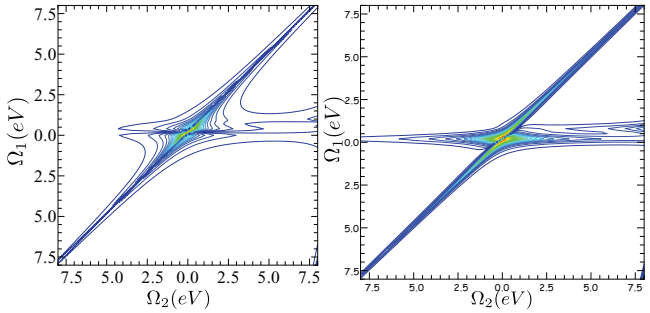

FIG. 5. (a) Optical potential (Eq. (21)) for the model system of Fig. 4, at Raman Resonances for four wave mixing with two frequencies ω_1 and ω_2 ($\Omega_1 = \omega_1$, $\Omega_2 = \omega_1 - \omega_2$; $\Omega_3 = 2\omega_1 - \omega_2$) with, $\mu_{ac} = 6D$, $\mu_{bc} = 1D$, $\omega_{ac} = 0.2014\,eV$, $\omega_{bc} = 20\,eV$, $\omega_{ba} \approx 20\,eV$, $\omega_{bb'} \approx 0eV$; $\eta_{ab} = 0.1\,\mathrm{cm}^{-1}$ and $\eta_{ac} = 0.2\,\mathrm{cm}^{-1}$. (b) Total Heterodyne signal for the same parameters by changing $\Re$ to $\Im$ in Eq. (21).

are given by

$$\mathbf{V}^{(n)}(\mathbf{r};t_j) = -\Re\hbar^{(-n)}\left[\int dt\mathbf{P}^{(n)}(t).\mathbf{E}^*(\mathbf{r},t)\right]$$
$$S^{(n)}_{het}(\mathbf{r};t_j) = -\frac{2^n}{\hbar^n}\Im\left[\int dt\mathbf{P}^{(n)}(t).\mathbf{E}^*(\mathbf{r},t)\right]. \quad (22)$$

Signals are now parameterized by the time delays between pulses t_1, t_2, t_3 rather than their frequencies. We can write the optical potential and corresponding heterodyne signals, to first order,

$$\mathbf{V}^{(1)}(\mathbf{r};t_1) = -\Re\left[\int dt\int_0^\infty d\tau_1 S^{(1)}(\tau_1)\mathbf{E}^*(t)\mathbf{E}(\tau_1)\right]$$
$$S^{(1)}_{het}(\mathbf{r};t_1) = -\Im\left[\int dt\int_0^\infty d\tau_1 S^{(1)}(\tau_1)\mathbf{E}^*(t)\mathbf{E}(\tau_1)\right], \quad (23)$$

in second order,

$$\mathbf{V}^{(2)}(\mathbf{r};t_1,t_2) = -\Re\left[\int dt\int_0^\infty d\tau_1\int_0^\infty d\tau_2 S^{(2)}(\tau_1,\tau_2)\right.$$
$$\left.\mathbf{E}_1(\tau_1)\mathbf{E}_2(\tau_2)\mathbf{E}_3^*(t)\right]$$
$$S^{(2)}_{het}(\mathbf{r};t_1,t_2) = -\Im\left[\int dt\int_0^\infty d\tau_1\int_0^\infty d\tau_2 S^{(2)}(\tau_1,\tau_2)\right.$$
$$\left.\mathbf{E}_1(\tau_1)\mathbf{E}_2(\tau_2)\mathbf{E}_3^*(t)\right], \quad (24)$$

finally, in third order,

$$\mathbf{V}^{(3)}(\mathbf{r};t_1,t_2,t_3)$$
$$= -\Re\left[\int dt\int_0^\infty d\tau_1\int_0^\infty d\tau_2\int_0^\infty d\tau_3\right.$$
$$\left.S^{(3)}(\tau_3,\tau_2,\tau_1)\mathbf{E}_4^*(t)\mathbf{E}_1(\tau_1)\mathbf{E}_2^*(\tau_2)\mathbf{E}_3(\tau_3)\right] \quad (25)$$

$$S^{(3)}_{het}(\mathbf{r};t_1,t_2,t_3)$$
$$= -\Im\left[\int dt\int_0^\infty d\tau_1\int_0^\infty d\tau_2\int_0^\infty d\tau_3\right.$$
$$\left.S^{(3)}(\tau_3,\tau_2,\tau_1)\mathbf{E}_4^*(t)\mathbf{E}_1(\tau_1)\mathbf{E}_2^*(\tau_2)\mathbf{E}_3(\tau_3)\right]. \quad (26)$$

We again focus on vibrational resonances and assume electronically off-resonant frequencies. For $\chi^{(2)}$ (Fig. 2), if we have two temporally resolved impulsive electric fields with delay t_1 and total phase $\sum_i^n \phi_i = 0$, we can then write the $\mathbf{P}^{(2)}(\mathbf{r},t_1)$ as[26–28]

$$\mathbf{P}^{(2)}(\mathbf{r},t_1) = \mathcal{E}_1\mathcal{E}_2\sum_a P(a)\mu_{ab}|\mu_{ca}|^2 I_{ac}(t_1)e^{i\omega_1 t_1}, \quad (27)$$

where we define, $P(a) = e^{-\beta\varepsilon_a}/\sum_a e^{-\beta\varepsilon_a}$ and $I_{vv'}(t) = exp[-i\omega_{vv'}t_1 - \gamma_{vv'}t_1]$. For simplicity, the r dependence is engraved in the envelope $\mathcal{E}$ and has not been explicitly written. Now we can write the second order optical potential measured as a function of t at $t = t_1$ with $t_2 = 0$ as,

$$\mathbf{V}^{(2)}(\mathbf{r},t_1) = \Re\hbar^{(-2)}\left[i\mathcal{E}_1\mathcal{E}_2\mathcal{E}_3^*\sum_a P(a)\mu_{ac}\mu_{cb}\mu_{bc}|I_{ac}(t_1)|^2 e^{i\omega_1 t_1}\right]. \quad (28)$$

Heterodyne signals are given by replacing $\Re$ in Eqs. (28) and (29) with $\Im$. One could observe the Raman resonance at conjugate frequency (Ω_1) by Fourier transforming Eq. (28) with respect to t_1 as

$$\mathbf{V}^{(2)}(\mathbf{r},\Omega_1) = \int_0^\infty dt_1\mathbf{V}^{(2)}(\mathbf{r},t_1)e^{i\Omega_1 t_1}. \quad (29)$$

For three temporally separated electric fields (Fig. 4), we assume that the field envelopes $\mathcal{E}_i(t)$ does not allow matter to evolve during the pulse and the fields are long enough so that their spectral bandwidth is narrow enough to show vibrational Raman resonances. Using coherent ($\sum_i^n \phi_i = 0$) and impulsive ($\mathcal{E}_i(t) = \mathcal{E}_i\delta(t)$) fields, we can immediately write the Raman resonance term for optical potential using loop diagrams in Fig. 4 and Eq. (25), as Eq. (30),

$$\mathbf{V}^{(3)}(\mathbf{r},t_2) = \Re\left[\frac{-1}{\hbar^3}|\mathcal{E}_1|^2|\mathcal{E}_2^*|^2\sum_a P(a)|\mu_{ab}|^2|\mu_{ca}|^2\right.$$
$$\left.|I_{ca}(t_2)|^2 e^{i(\omega_1-\omega_2)t_2}\right]. \quad (30)$$

The heterodyne-detected signal corresponding to Eq. (30) is obtained by simply replacing $\Re$ in Eq. (30) with $\Im$. If we Fourier transform Eq. (30), similar to Eq. (29), but with respect to t_2 using conjugate frequency (Ω_2) instead, we can observe the vibrational Raman resonance at $\Omega_2 = \omega_{ac}$. In our case, this will give a similar optical potential and heterodyne-detected signal as shown in Fig. 6 for $\chi^{(2)}$ processes but with a different prefactor. Since we considered electronically off-resonant processes, second and third order optical potentials can simply be parameterized by conjugate frequencies Ω_1 or Ω_2 respectively, as in Eqs. (29) and (30), giving one dimensional spectra. When extended to electronically resonant system, one would be able to get

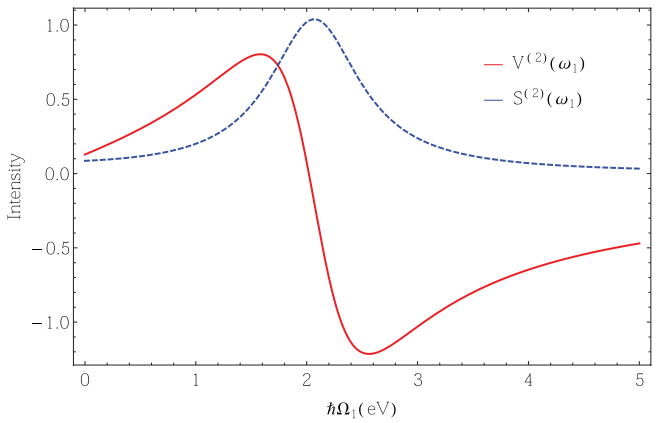

FIG. 6. Time resolved $\chi^{(2)}$ (Eqs. (28) and (29)) with similar parameters as Fig. 3.

multidimensional time-domain spectra with variable pulse delays.

In summary, we showed that AFM detection closely resembles coherent heterodyne signals with appropriate phase matching. This is in contrast with other incoherent detection techniques like Florescence,[15] photo-acoustic,[19,20] and photoelectron detection.[21]

The authors wish to thank H. K. Wickramasinghe and E. Potma for useful discussions. They gratefully acknowledge the support of the Chemical Sciences, Geosciences and Biosciences Division, Office of Basic Energy Sciences, Office of Science, U.S. Department of Energy. In addition, they also thank the National Science Foundation (Grant No. CHE-1058791) and the National Institute of Health (Grant No. GM-59230) for their support.

[1]T. Plakhotnik, E. A. Donley, and U. P. Wild, Annu. Rev. Phys. Chem. **48**, 181 (1997).
[2]S. Mukamel, D. Healion, Y. Zhang, and J. D. Biggs, Annu. Rev. Phys. Chem. **64**, 101 (2013).
[3]M. B. Dahan, E. Peik, J. Reichel, Y. Castin, and C. Salomon, Phys. Rev. Lett. **76**, 4508 (1996).
[4]J. Zhang, P. Chen, B. Yuan, W. Ji, Z. Cheng, and X. Qiu, Science **342**, 611 (2013).
[5]K. C. Neuman and A. Nagy, Nat. Methods **5**, 491 (2008).
[6]S. Kasas, N. Thomson, B. Smith, P. Hansma, J. Miklossy, and H. Hansma, Int. J. Imaging Syst. Technol. **8**, 151 (1997).
[7]J. Yan, D. Skoko, and J. F. Marko, Phys. Rev. E **70**, 011905 (2004).
[8]S. C. Kuo and M. P. Sheetz, Science **260**, 232 (1993).
[9]S. Hohng, S. Lee, J. Lee, and M. H. Jo, Chem. Soc. Rev. **43**, 1007 (2014).
[10]M. Orrit, T. Ha, and V. Sandoghdar, Chem. Soc. Rev. **43**, 973 (2014).
[11]D. Kilinc and G. U. Lee, Integr. Biol. **6**, 27 (2014).
[12]T. Kudo and H. Ishihara, Phys. Chem. Chem. Phys. **15**, 14595 (2013).
[13]I. Rajapaksa, K. Uenal, and H. K. Wickramasinghe, Appl. Phys. Lett. **97**, 073121 (2010).
[14]A. E. Cohen and S. Mukamel, J. Phys. Chem. A **107**, 3633 (2003).
[15]S. Mukamel and M. Richter, Phys. Rev. A: At., Mol., Opt. Phys. **83**, 013815 (2011).
[16]G. Roumpos and S. T. Cundiff, JOSA B **30**, 1303 (2013).
[17]D. Brinks, F. D. Stefani, F. Kulzer, R. Hildner, T. H. Taminiau, Y. Avlasevich, K. Müllen, and N. F. Van Hulst, Nature (London) **465**, 905 (2010).
[18]D. Brinks, R. Hildner, E. M. van Dijk, F. D. Stefani, J. B. Nieder, J. Hernando, and N. F. van Hulst, Chem. Soc. Rev. **43**, 2476 (2014).
[19]G. A. West, J. J. Barrett, D. R. Siebert, and K. V. Reddy, Rev. Sci. Instrum. **54**, 797 (1983).
[20]S. Y. Emelianov, P.-C. Li, and M. O'Donnell, Phys. Today **62**, 34 (2009).
[21]H. Cohen, Appl. Phys. Lett. **85**, 1271 (2004).
[22]I. Rajapaksa and H. K. Wickramasinghe, Appl. Phys. Lett. **99**, 161103 (2011).
[23]T. Iida and H. Ishihara, Phys. Rev. Lett. **97**, 117402 (2006).
[24]S. Mukamel, *Principles of Nonlinear Optical Spectroscopy* (Oxford University Press New York, 1995), Vol. 29.
[25]S. Rahav and S. Mukamel, Proc. Natl. Acad. Sci. U.S.A. **107**, 4825 (2010).
[26]J. Y. Huang and Y. Shen, Phys. Rev. A **49**, 3973 (1994).
[27]S. Roke, A. W. Kleyn, and M. Bonn, Chem. Phys. Lett. **370**, 227 (2003).
[28]I. V. Stiopkin, H. D. Jayathilake, A. N. Bordenyuk, and A. V. Benderskii, J. Am. Chem. Soc. **130**, 2271 (2008).